RSC Advances

PAPER

View Article Online
View Journal | View Issue

Cite this: *RSC Adv.*, 2018, **8**, 1132

Controlled synthesis of brightly fluorescent $CH_3NH_3PbBr_3$ perovskite nanocrystals employing $Pb(C_{17}H_{33}COO)_2$ as the sole lead source†

Xiaoming Fu, ‡[ac] Zhiwei Peng, ‡[b] Chi Zhang,[a] Yong Xia,[a] Jianbing Zhang,[a] Wei Luo,[ae] L. Jay Guo,[e] Honglang Li,*[d] YuHuang Wang*[b] and Daoli Zhang*[ab]

Organometal halide perovskite nanocrystals hold vast potential for application in photovoltaics, light emitting diodes, low-threshold lasers, and photodetectors due to their size-tunable bandgap energies and photoluminescence as well as excellent electron and hole mobilities. However, the synthesis of such nanocrystals typically suffers from poor structural stability in solution and the coexistence of lamellate nanocrystals (nanoplatelets) and spherical nanocrystals (nanoparticles). Here we show that the pure nanoparticle morphology of $CH_3NH_3PbBr_3$ nanocrystals can be realized by employing lead oleate ($Pb(C_{17}H_{33}COO)_2$) as the sole lead source and controlled using short- and long-chain mixed alkyl ammonium. These nanocrystals are monodispersed (2.2 ± 0.4 nm in diameter), highly fluorescent (with a quantum yield approaching 85%), and highly stable in the solution (for more than 30 days). Comparative studies reveal that the shape of $CH_3NH_3PbBr_3$ nanocrystals is strongly dependent on the lead source, $PbBr_2$ and $Pb(C_{17}H_{33}COO)_2$, and evolves as a function of the ratio of short- and long-chain alkyl ammoniums in the precursors. At an optimal short to long-chain alkyl ammonium ratio of 4 : 6, the growth of $CH_3NH_3PbBr_3$ nanoplatelets can be selectively suppressed with $Pb(C_{17}H_{33}COO)_2$ as the sole lead source, enhancing the overall photoluminescence quantum yield of the produced $CH_3NH_3PbBr_3$ nanocrystals. This work reveals important new insights for controlled synthesis of perovskite nanocrystals with pure crystal shape and significantly improved photoluminescence properties and stability.

Received 27th October 2017
Accepted 19th December 2017

DOI: 10.1039/c7ra11832e

rsc.li/rsc-advances

Introduction

Organolead halide perovskites (OHP) are intensively researched for photovoltaics because of their high light conversion efficiency,[1,2] optimal bandgap energy[3,4] and excellent electron and hole mobilities.[5,6] These compounds, possessing a general formula of $APbX_3$ crystal structure (A = organic ammonium cation and X = halide anion), have been applied to solar cells and led to a breakthrough performance in photovoltaic power conversion efficiencies from 3.1% (ref. 8) in 2009 to a certified 22.7% now.[9] In addition to solar energy harvesting, the size-tunable bandgap energies and photoluminescence (PL) from perovskite materials also evoke the exploration of their potential uses as emission materials by decreasing the particle size to nanocrystals (NCs). With nanoscaled size, OHP NCs have sharp excitonic features, which provide a synthetically tunable system for systematic investigations of the nature and dynamics of the excited states of OHP.[10] In the 1990s, Papavassiliou *et al.* systematically investigated the structure, optical and other related properties of OHP NCs,[11,12] in which the high photoluminescence quantum yield (PLQY) and large exciton binding energy offered interesting opportunities for application in field-effect transistors (FET) and light emitting diodes (LEDs).[13,14]

In 2014, OHP NCs captured the attention of researchers again when Schmidt *et al.*[15] synthesized 6 nm-sized $CH_3NH_3PbBr_3$ perovskite NCs *via* a simple solution process. In their experiments, lead bromide ($PbBr_2$), methylammonium bromide (MABr) and octylammonium bromide (OABr) were added to a stirring solution of oleic acid (OLA) and 1-octadecene (ODE) at 80 °C and the reaction was quenched by injecting acetone quickly. It is believed that the long alkyl chain cations acted as the capping ligands of the NCs to restrict the growth of the $CH_3NH_3PbBr_3$ array extending in three dimensions. Subsequent research found that two-dimensional nanoplatelets of

[a]*School of Optical and Electronic Information, Huazhong University of Science and Technology, 1037 Luoyu Road, Hongshan District, Wuhan City, Hubei Province, 430074, P. R. China. E-mail: zhang_daoli@hust.edu.cn*

[b]*Department of Chemistry and Biochemistry, University of Maryland, 8051 Regent Drive, College Park, MD 20742, USA. E-mail: yhw@umd.edu*

[c]*School of Physics, Communication and Electronics, Jiangxi Normal University, 99 Ziyang Avenues, Nanchang City, Jiangxi Province, 330022, P. R. China*

[d]*Institute of Acoustics, Chinese Academy of Sciences, 21 North 4th Ring Road, Haidian District, Beijing 100190, P. R. China. E-mail: lhl@mail.ioa.ac.cn*

[e]*Department of Electrical Engineering and Computer Science, University of Michigan, Ann Arbor, MI 48109, USA*

† Electronic supplementary information (ESI) available. See DOI: 10.1039/c7ra11832e

‡ These authors contribute equally to this work.

organolead bromide perovskites coexisted with nanoparticles in the synthesis.[16] Later on, a large number of experiments based on the solution process were carried out and these OHP NCs with higher PLQY were applied to novel optical devices.[17–20] However, these OHP NCs are unstable in solution and the structures are heterogeneous,[21] with different crystal shapes including nanoparticles and nanoplatelets coexisting as mixtures. Light emitting devices require phosphors with high PLQY and narrow-band emissions.[22] The coexistence of $CH_3NH_3PbBr_3$ nanoplatelets and nanoparticles hampers applications in practical optical devices because they behave different PL emission peaks and PLQY. From a synthetic point of view, when using inorganic $PbBr_2$ as the lead precursor, $CH_3NH_3PbBr_3$ nanoplatelets will form by intercalation of guest organic moieties between the Pb–Br–Pb layers of the crystalline $PbBr_2$ host,[23] implying that the formation of $CH_3NH_3PbBr_3$ nanoplatelets would be suppressed if $PbBr_2$ is replaced by other precursors as lead sources.

In the present work, we developed a facile method to synthesize monodispersive and stable $CH_3NH_3PbBr_3$ perovskite NCs using lead oleate ($Pb(C_{17}H_{33}COO)_2$, Pb-oleate) as the sole lead source and ligand to replace $PbBr_2$ and OLA in the precursors. The resulting $CH_3NH_3PbBr_3$ NCs showed pure and monodispersive nanoparticle structure with an average size of 2.2 nm, improved PLQY of 85%, and higher stability than those employing $PbBr_2$ as lead source and OLA or Pb-oleate as ligand. Our investigation further revealed that the mole ratios of long- and short-chain alkyl ammonium halides (OA^+ : MA^+) in the precursors can significantly affect the crystalline structures of $CH_3NH_3PbBr_3$ NCs toward nanoparticles and nanoplatelets with different layers *via* the quantum confinement effect. At an optimal OA^+ : MA^+ ratio of 4 : 6 with Pb-oleate as the sole lead source, the growth of nanoplatelets was essentially suppressed, generating pure $CH_3NH_3PbBr_3$ nanoparticles with enhanced optical properties. Comparative studies also verified that the nanoplatelet structure lowered the overall quantum yields of $CH_3NH_3PbBr_3$ NCs. To the best of our knowledge, this is the first report obtaining pure monodispersive $CH_3NH_3PbBr_3$ nanoparticles with favourable stability and good dispensability using Pb-oleate as the sole lead source in the reactants, and the results shown here may pave the way for further application of OHP NCs in optoelectronic devices.

Experimental section

Chemicals

Lead(II) oxide (PbO, 99.9%, Alfa), lead(II) bromide ($PbBr_2$, 99%, Aladdin), methylamine (CH_3NH_2, 33 wt% in absolute ethanol, Aladdin), hydrobromic acid (HBr, 48 wt% in water, Aladdin), *N*, *N*-dimethylformamide (DMF, anhydrous, 99.8%, Alfa), oleic acid (OLA, ≥99%, Sigma-Aldrich), 1-octadecene (ODE, >90%, Sigma-Aldrich) and *n*-octylamine (OA, $C_8H_{17}NH_2$, 99%, Aladdin). All the chemicals were used as received without further purification.

Synthesis of alkylammonium bromide

Alkylammonium bromide was synthesized by reaction between alkyl amine (CH_3NH_2 or $C_8H_{17}NH_2$) and HBr. Briefly, hydrobromic acid (5 mL, 44 mmol) was added to a solution of excess methylamine (12 mL, 96 mmol) in ethanol (50 mL) or slight less *n*-octylamine (7 mL, 42 mmol) at 0 °C. The mixture was continuously stirred for 4 h at 0 °C. Crystallization of alkylammonium bromide (MABr or OABr) was achieved using a rotary evaporator and washed three times with diethyl ether. The resulting powder was dried under vacuum (60 °C, 12 h) for future use.

Synthesis of Pb-oleate

The reaction was performed on a Schlenk line using standard air-free techniques. In a typical synthesis, 3 mmol PbO, 7.5 mmol OLA and 30 mL ODE were mixed in a 150 mL flask, and then heated to 120 °C for 1 h under vacuum to obtain a clear solution, followed by natural cooling to the ambient temperature under N_2 blow protection. The solution was then quenched using acetone and the precipitates were redispersed in toluene to a concentration of 0.4 mol L^{-1}.

Synthesis of hybrid $CH_3NH_3PbBr_3$ NCs using $PbBr_2$ and Pb-oleate as lead sources

Stock solutions of $PbBr_2$ and MABr, with the same concentration 0.5 mol L^{-1}, were prepared in DMF. The solution of lead source was prepared by mixing the same mole of $PbBr_2$–DMF and Pb-oleate–toluene solutions. The alkyl ammonium halides were prepared in DMF, and the molar ratios of OABr and MABr were tuned as 9 : 1, 7 : 3, 6 : 4, 5 : 5, 4 : 6, 3 : 7, and 1 : 9. Then the reagents were mixed to obtain a series of precursor solutions with fixed total mole mass of $PbBr_2$ (4 mmol), alkyl ammonium bromides (4 mmol) and Pb-oleate (4 mmol). To obtain the desired perovskite crystallization, the precursor solution was added dropwise into 10 mL toluene under vigorous stirring at 80 °C. After centrifugation at 7000 rpm for 10 min to discard the precipitates, a bright yellow-green suspension or blue suspension was obtained because of different proportions of nanoplatelets and nanoparticles in solution. The solution of hybrid perovskite NCs was filtered using a polytetrafluoroethylene (PTFF) syringe filter (pore size 0.45 μm).

Synthesis of hybrid $CH_3NH_3PbBr_3$ NCs using $PbBr_2$ and OLA

Except for using OLA to replace Pb-oleate in the precursors, the synthesis scheme is similar to the synthesis of hybrid $CH_3NH_3PbBr_3$ NCs using $PbBr_2$ and Pb-oleate as lead sources.

Synthesis of pure $CH_3NH_3PbBr_3$ nanoparticles

The precursor solution was prepared by mixing the Pb-oleate–toluene solution (4 mmol) and the alkyl ammonium bromides (4 mmol) with an OA^+ : MA^+ ratio of 4 : 6. To obtain the desired pure perovskite nanoparticles, the precursor solution was added into 10 mL toluene quickly under vigorous stirring at 80 °C. After centrifugation at 7000 rpm for 10 min to discard the precipitates, a bright green suspension was obtained, which was filtered using a polytetrafluoroethylene (PTFF) syringe filter (pore size 0.45 μm). Finally, there was nearly 100% chemical

yield of the small $CH_3NH_3PbBr_3$ perovskite nanoparticles using Pb-oleate as sole lead source and an OA^+ : MA^+ ratio of 4 : 6.

It is noted that the above-mentioned synthesis of $CH_3NH_3PbBr_3$ nanoparticles can be scaled up. In addition, if only the two DMF solutions of $PbBr_2$ and MABr in 1 : 1 ratio were employed in the absence of any ligands in the synthesis system and then dropped into 10 mL of anhydrous toluene under vigorous stirring, $CH_3NH_3PbBr_3$ would precipitate out as bulk crystals.

Characterization of $CH_3NH_3PbBr_3$ NCs

The UV-vis absorption was recorded using UV-3600 plus of Shimadzu corporation and PL emission was collected in air using F-280 of Tianjin Gangdong Science & Technology Co. Ltd. Relative quantum yield measurements were taken using a 0.5 mol L^{-1} quinine sulphate as a reference and exciting at 336 nm. $CH_3NH_3PbBr_3$ NCs samples in toluene were deposited on amorphous carbon-coated copper grids, and the morphology of the samples was investigated using an FEI Tecnai G2 20 or a JEM 2100 TEM operating at 200 kV for images of transmission electron microscopy (TEM). The solid colloidal NCs were obtained by fast evaporating the toluene on a hot plate at 80 °C. The X-ray diffraction (XRD) patterns were obtained on X'Pert PROX-ray diffractometer from PANalytical B.V. equipped with Cu K_α radiation. The samples were scanned from $5° < 2\theta < 50°$ in 5 min.

PLQY was calculated by the following formula:

$$\eta_P = \frac{S_P}{S_Q} \times \eta_Q$$

where η_P and η_Q represent PLQY of $CH_3NH_3PbBr_3$ NCs and quinine sulfate, while S_P and S_Q represent the photoluminescence integral area of $CH_3NH_3PbBr_3$ NCs and quinine sulfate, respectively.

Result and discussion

To investigate the impact of lead sources and ligand on the structure of produced $CH_3NH_3PbBr_3$ NCs, we used Pb-oleate, $PbBr_2$ + Pb-oleate, and $PbBr_2$ + OLA in the precursors with an fixed OA^+ : MA^+ ratio of 4 : 6, and the morphology of the synthesized $CH_3NH_3PbBr_3$ NCs were first examined by TEM with an average diameter of 2.2 nm and a deviation of ±0.4 nm (Fig. 1d). High-resolution TEM image in Fig. 1b revealed that these nanoparticles are crystalline with a measured *d*-spacing of 2.6 Å. Together with the corresponding FFT pattern as shown in Fig. 1c, the exposing crystal facet was determined as (210). On the contrary, if $PbBr_2$ together with Pb-oleate was used as lead sources, the synthesized perovskite NCs showed a mixture of nanoparticles and nanoplatelets (Fig. 1e). When Pb-oleate was used as sole lead source and ligand in the reaction, the resulting perovskite NCs showed a monodispersed nanoparticle structure (Fig. 1a). Obviously, the use of inorganic lead source ($PbBr_2$) promoted the growth of $CH_3NH_3PbBr_3$ NCs in the nanoplatelet formation with larger size than nanoparticles, possibly due to less amount of size-confining organo attachments at the crystal edges. As an additional control, $PbBr_2$ + OLA was also utilized as the lead source and ligand in the precursors, however the

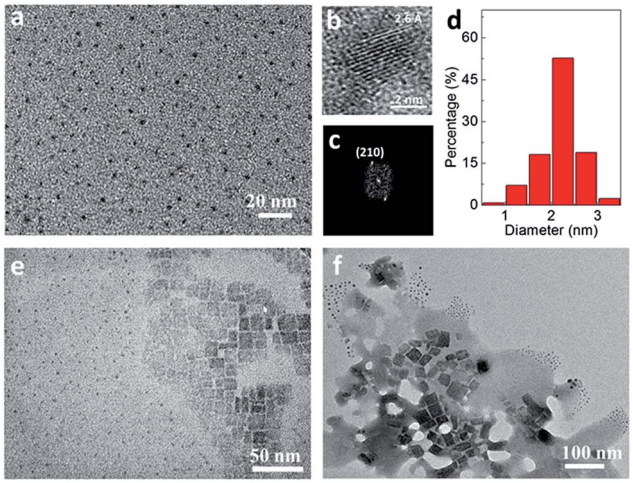

Fig. 1 Morphology of $CH_3NH_3PbBr_3$ NCs synthesized from different lead sources at OA^+ : MA^+ ratio of 4 : 6. (a) The TEM image of monodispersed $CH_3NH_3PbBr_3$ nanoparticles synthesized from Pb-oleate as sole Pb source. (b) The HRTEM image of an individual, crystalline $CH_3NH_3PbBr_3$ nanoparticle. (c) Corresponding FFT pattern of the HRTEM image in (b). (d) Size distribution of monodispersed $CH_3NH_3PbBr_3$ nanoparticles. (e) TEM image of $CH_3NH_3PbBr_3$ NCs synthesized from Pb-oleate + $PbBr_2$ as Pb source. It shows a mixture of nanoplatelets and nanoparticles. (f) TEM image of $CH_3NH_3PbBr_3$ NCs synthesized from OLA + $PbBr_2$ as Pb source.

produced $CH_3NH_3PbBr_3$ NCs presented a mixture of small-sized and large-sized cubic nanoparticles in addition with a thick organic cluster layers surrounding $CH_3NH_3PbBr_3$ NCs. Additionally, the $CH_3NH_3PbBr_3$ NCs synthesized from Pb-oleate were stable in toluene solution under ambient air conditions up to 30 days, but the ones from $PbBr_2$ + OLA or $PbBr_2$ + Pb-oleate gradually aggregated and precipitated out from the solution during the same period. The observed differences on the morphology and stability of the produced $CH_3NH_3PbBr_3$ NCs suggests that (1) OLA as a ligand cannot effectively integrate with the $CH_3NH_3PbBr_3$ NCs, and produces undesired organic impurities that embed the $CH_3NH_3PbBr_3$ NCs; (2) the use of inorganic $PbBr_2$ as lead source results in the co-production of both nanoplatelets and nanoparticles; and (3) the use of Pb-oleate as both sole lead source and ligand can effectively restrain the growth of $CH_3NH_3PbBr_3$ nanoplatelets, producing pure $CH_3NH_3PbBr_3$ nanoparticles with ultra-small sizes, narrow size distribution and higher stability. It is possible that during the formation of $CH_3NH_3PbBr_3$ NCs when using Pb-oleate as sole lead source, $C_{17}H_{33}COO^-$ ion from Pb-oleate was effectively coordinate at the surface of $CH_3NH_3PbBr_3$ NCs, confining the nanocrystal size and enhancing the stability of $CH_3NH_3PbBr_3$ NCs. When $PbBr_2$ was added into the reaction, guest organic moieties intercalated between the Pb–Br–Pb layers of the crystalline $PbBr_2$ host forming $CH_3NH_3PbBr_3$ nanoplatelets.

The structure and crystallinity of $CH_3NH_3PbBr_3$ NCs synthesized from three different precursors were further investigated with XRD (Fig. 2). Here, bulk $CH_3NH_3PbBr_3$ was also synthesized without the help of ligand and compared as reference. For the $CH_3NH_3PbBr_3$ NCs synthesized from Pb-

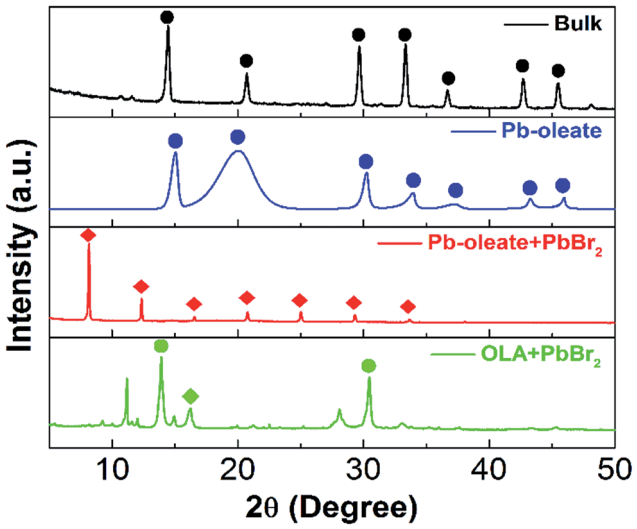

Fig. 2 XRD patterns of $CH_3NH_3PbBr_3$ bulk powders (black) and NCs synthesized from Pb-oleate (blue), Pb-oleate + $PbBr_2$ (red) and OLA + $PbBr_2$ (green) as lead source (● bulk unit cell, ◆ nanoplatelets stacks).

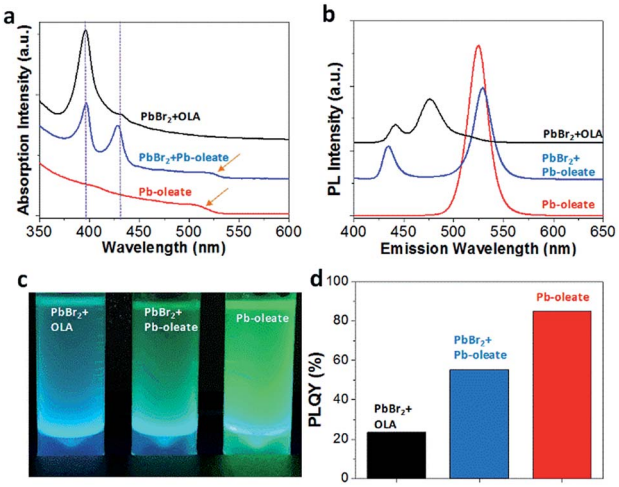

Fig. 3 Optical properties of $CH_3NH_3PbBr_3$ NCs synthesized from different lead sources at OA^+ : MA^+ ratio of 4 : 6. (a) Absorption curves of $CH_3NH_3PbBr_3$ NCs synthesized from OLA + $PbBr_2$ (black), Pb-oleate + $PbBr_2$ (blue) and Pb-oleate (red) as lead source. The curves were offset for better comparison. (b) PL emission of $CH_3NH_3PbBr_3$ NCs synthesized from OLA + $PbBr_2$ (black), Pb-oleate + $PbBr_2$ (blue) and Pb-oleate (red) as lead source. The excitation wavelength was set at 350 nm. The curves were offset for better comparison. (c) Pictures of three $CH_3NH_3PbBr_3$ NCs in toluene solutions taken under 365 nm laser illumination. (d) Quantum yield comparison of three $CH_3NH_3PbBr_3$ NCs in toluene solutions.

oleate + $PbBr_2$, a series of diffraction peaks at 8.2°, 12.4°, 16.5°, 20.8°, 25.0°, 29.3°, and 33.7° were detected representing the layered diffractions of $CH_3NH_3PbBr_3$ nanoplatelets stacking in the sample.[24] These diffraction peaks were at a regular interval of ~4.2°, which corresponds to an average spacing of ~2.1 nm between the layers in these nanoplatelets.[24,25] The observation of higher order peaks also testified that $CH_3NH_3PbBr_3$ nanoplatelets are well crystallized. Due to much larger size of nanoplatelet than nanoparticles as revealed previous in the TEM image (Fig. 1e), the diffraction peaks from nanoplatelets in this sample were so dominating that any peaks from nanoparticles were almost negligible. With $PbBr_2$ + OLA as lead source and ligand, the series layered diffraction peaks of $CH_3NH_3PbBr_3$ nanoplatelets were absent while the diffraction peaks of bulk unit cell became preeminent, indicating that large-sized and crystalline $CH_3NH_3PbBr_3$ nanoparticles were formed. When Pb-oleate was used both as sole lead source and ligand, the diffraction peak positions from the nanoparticles showed up and correlated well with the bulk $CH_3NH_3PbBr_3$ with a much broader peak width, verifying the nanoparticle structure with ultra-small size in the sample. Also, the absence of series layered diffraction peaks from nanoplatelets indicates the high purity of $CH_3NH_3PbBr_3$ NCs in the nanoparticle structure. A summary of XRD peaks and calculated *d*-space of the as-synthesized $CH_3NH_3PbBr_3$ NCs from Pb-oleate and its comparison to bulk $CH_3NH_3PbBr_3$ is shown in Table S1.†

With their distinct structure and morphology, these $CH_3NH_3PbBr_3$ NCs synthesized from different precursors also presented different optical properties (Fig. 3). The $CH_3NH_3PbBr_3$ NCs from OLA + $PbBr_2$ showed a dominated absorption peak at 396 nm and a small shoulder peak at 431 nm, corresponding to mono- and bi-layer $CH_3NH_3PbBr_3$ nanoplatelets (Fig. 3a).[11] When changing to Pb-oleate + $PbBr_2$, the peak at 431 nm for bi-layer $CH_3NH_3PbBr_3$ nanoplatelet became stronger, along with the appearance of an absorption peak from nanoparticles at around 520 nm as indicated by the orange arrow in Fig. 3a. Here, the higher absorption energy of nanoplatelets than nanoparticles is because of larger exciton binding energy.[11,19,26] As for Pb-oleate, the absorption peaks from nanoplatelets were disappeared, but the peak from nanoparticles remained, demonstrating again the pure nanoparticle morphology in this sample. PL emissions provide further evidence as shown in Fig. 3b. $CH_3NH_3PbBr_3$ NCs from OLA + $PbBr_2$ presented only peaks at 442 and 476 nm representing bi- and four-layer $CH_3NH_3PbBr_3$ nanoplatelets,[11] while $CH_3NH_3PbBr_3$ NCs from Pb-oleate + $PbBr_2$ showed both nanoplatelet peak at 434 nm and nanoparticle peak at 529 nm. As a comparison, the use of Pb-oleate as sole lead source resulted in only nanoparticle emission at 520 nm with no emissions from nanoplatelets. A picture of three solutions under UV 365 nm laser illumination was provided in Fig. 3c. The green colour in the samples synthesized from Pb-oleate and $PbBr_2$ + Pb-oleate clearly indicated the existence of $CH_3NH_3PbBr_3$ nanoparticles, in contrast with the one from $PbBr_2$ + OLA showing the blue colour. It is also worth noting that PLQY of $CH_3NH_3PbBr_3$ NCs from Pb-oleate as sole lead source were enhanced a factor of 2 and 4.3, respectively, compared to those from $PbBr_2$ + Pb-oleate and $PbBr_2$ + OLA, leading to an improved overall PLQY to 85% (Fig. 3d). Other than the type of lead sources, the amount of them also played an important role in determining the optical properties of $CH_3NH_3PbBr_3$ NCs. When changing the amount of Pb-oleate from 4 mmol, which is equivalent to the total amount of alkyl ammonium halides (OA^+ plus MA^+), to less (2 mmol) or more (7 mmol), the absorption as well as PL emission from $CH_3NH_3PbBr_3$ nanoparticles were significantly weakened (Fig. S1†), indicating the lower quality of the produced perovskite NCs.

To further investigate the growth mechanism of $CH_3NH_3PbBr_3$ NCs and control the morphology (nanoparticles or nanoplatelets), the ratios of long- and short-chain alkyl ammonium halides (OA^+ : MA^+) were varied (1 : 9, 3 : 7, 4 : 6, 5 : 5, 6 : 4, 7 : 3 and 9 : 1) in the precursors with Pb-oleate as sole lead source. At the starting OA^+ : MA^+ ratio of 1 : 9, a strong absorption peak at 425 nm representing bi-layer $CH_3NH_3PbBr_3$ nanoplatelets appeared while the absorption peak from $CH_3NH_3PbBr_3$ nanoparticles at ~520 nm was weak (Fig. 4a), indicating that the formation of nanoplatelets was dominated. With increasing percentage of OA^+ to 50% (OA^+ : MA^+ ratio of 5 : 5), the absorption peak of nanoplatelets quickly decreased to be negligible, and that of nanoparticles became noticeable, demonstrating the more favorable formation of nanoparticle structure. At increasing OA^+, the absorption peak of nanoplatelets reappears along with the decrease of nanoparticle absorption. Similar trends were also observed in PL emission as shown in Fig. 4b, where the nanoplatelet PL peak at around 440 nm followed by a U-shape with varying OA^+ : MA^+ ratios from 1 : 9 to 9 : 1. On the contrary, the nanoparticle PL (around 525 nm) peaks evolved in the opposite tendency, with lower intensity at larger OA^+ : MA^+ amount differences and higher intensity at even amount of OA^+ : MA^+. Interestingly, the overall PLQY of the solution followed the same tendency with nanoparticle PL intensity (Fig. 4d). Highest PLQY of 85% was achieved at an OA^+ : MA^+ ratio of 4 : 6 when PL peak intensity from nanoplatelets was the lowest and PL peak intensity from nanoparticles was the highest, again proving that the growth of $CH_3NH_3PbBr_3$ nanoplatelets needs to be suppressed in order to obtain the high PLQY. These PLQY values are consistent with previous reported on two-dimensional layered OHP NCs[27] and monodisperse OHP nanoparticles[28] obtained through different synthesis methods.

The growth mechanism of $CH_3NH_3PbBr_3$ NCs can be revealed by the schematic overview in Scheme 1. Generally speaking, during the growth of $CH_3NH_3PbBr_3$ NCs with both short-chain methylammonium (MA^+) and long-chain octylammonium (OA^+), the small MA^+ fits in the centre of eight $PbBr_6$ corner-shared octahedral, while the large OA^+ fits only the periphery of a set of four $PbBr_6$ octahedral in the formation of $CH_3NH_3PbBr_3$ NCs because of steric effects.[24,29,30] An interesting phenomenon aroused when a mixture of short and long organic cations was employed. While the small MA^+ entering the centre of $PbBr_6$ corner-shared octahedral tends to comfort the three-dimensional (3D) bulk perovskite structure, the long-chain cations (for example OA^+) occupying the position of the small MA^+ makes the 3D perovskite structure unsuitable and thus it breaks up into smaller sized perovskite NCs. When using inorganic $PbBr_2$ as the lead precursor, $CH_3NH_3PbBr_3$ NCs (including nanoparticles and nanoplatelets) will form by intercalation of the small MA^+ and large OA^+ between the Pb–Br–Pb layers of the crystalline $PbBr_2$ host (Scheme 1a). However, using Pb-oleate as sole lead source, $PbBr_6$ corner-shared octahedral, provided bromide source by alkylammonium bromide, are formed firstly, and then are assembled to OHP NCs which are capped with the ligands of fatty acid (Scheme 1b). If the ratios of long- and short-chain alkyl ammonium halides are suitable, the growth of nanoplatelets would be essentially suppressed, generating pure $CH_3NH_3PbBr_3$ nanoparticles with enhanced optical properties.

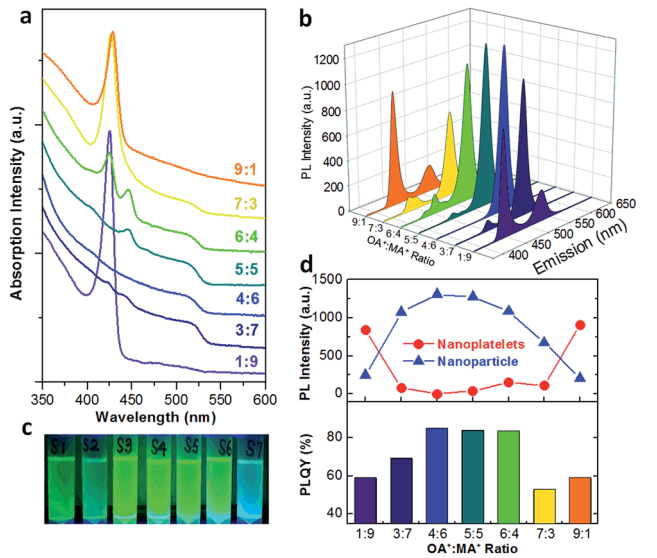

Fig. 4 Investigation of the impact of OA^+ : MA^+ ratios on the optical properties of the resulting $CH_3NH_3PbBr_3$ NCs solutions using Pb-oleate as sole lead source. (a) UV-vis absorption curves of as-made $CH_3NH_3PbBr_3$ NCs solutions with varying OA^+ : MA^+ ratios. The curves were offset for better comparison. (b) PL emissions of as-made $CH_3NH_3PbBr_3$ NCs solutions with varying OA^+ : MA^+ ratios. The excitation wavelength was set as 350 nm. (c) Picture of $CH_3NH_3PbBr_3$ NCs solutions synthesized from varying OA^+ : MA^+ ratios taken under UV light. The samples labeled from S1 to S7 represent different OA^+ : MA^+ ratios from 1 : 9 to 9 : 1. (d) The overall PLQY of as-made $CH_3NH_3PbBr_3$ NCs solutions and respective PL peak intensity of nanoplatelets and nanoparticles with varying OA^+ : MA^+ ratios.

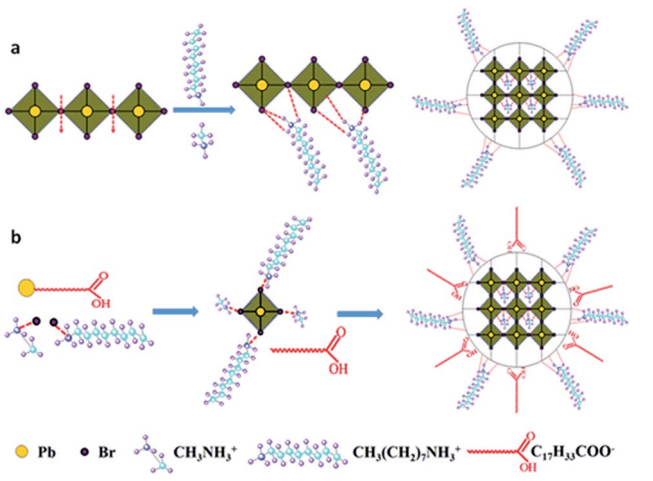

Scheme 1 Schematic overview of the grow mechanism of $CH_3NH_3PbBr_3$ NCs. (a) $CH_3NH_3PbBr_3$ NCs (including nanoparticles and nanoplatelets) are both formed by intercalation of the small MA^+ and large OA^+ between the Pb–Br–Pb layers of the crystalline $PbBr_2$ host using inorganic $PbBr_2$ as the lead precursor. (b) Pure $CH_3NH_3PbBr_3$ nanoparticles are obtained at an optimal OA^+ : MA^+ ratio of 4 : 6 with Pb-oleate as the sole lead source, suppressing the growth of nanoplatelets.

To further analyse the impact of $OA^+ : MA^+$ ratio on PL properties of $CH_3NH_3PbBr_3$ nanoparticles, the position and full width at half maximum (FWHM) of PL peaks of $CH_3NH_3PbBr_3$ nanoparticles were summarized in Fig. S2.† We observed a blue shift of PL peak of $CH_3NH_3PbBr_3$ nanoparticles from 527 nm to 516 nm with increasing the ratio of $OA^+ : MA^+$, indicating a decreased nanoparticle size. This observation also proves the concept that the longer alkyl chain (OA^+) restricts the 3D growth of $CH_3NH_3PbBr_3$ nanoparticles and thus strengthens the nano-size quantum confinement effect. At $OA^+ : MA^+$ ratios ranging from 3 : 7 to 7 : 3, FWHM was below 24 nm, showing narrow size distribution of $CH_3NH_3PbBr_3$ nanoparticles and in agreement with previous TEM imaging results (Fig. 1). The emission colours of different species under 365 nm laser illumination were illustrated in Fig. 4c. Considering all factors, the optimal growth conditions for monodispersed $CH_3NH_3PbBr_3$ NCs were determined using Pb-oleate as sole lead source and an $OA^+ : MA^+$ ratio of 4 : 6, from which highly fluorescent $CH_3NH_3PbBr_3$ nanoparticles could be synthesized as the potential phosphors in LEDs.

We further studied the impact of alkyl ammonium halides on the formation of $CH_3NH_3PbBr_3$ perovskite NCs using $PbBr_2$ and Pb-oleate as lead sources. As shown in Fig. 5a and b, in general the absorption and emission peaks from nanoparticles at around 520 nm followed similar trends when using Pb-oleate as sole lead source in which the intensity increased first and then decreased along with increasing $OA^+ : MA^+$ ratios. This indicated that an even OA^+/MA^+ amount would promote the growth of perovskite NCs in nanoparticle formation even with $PbBr_2$ as lead source. Although the exact position of absorption peak from nanoparticles was hard to be recognized, the blue-shifting effect was clearly observed as indicated by the red dashed arrow in Fig. 5a. Similarly, PL emission position of nanoparticles was blue-shifted from 528 nm at the $OA^+ : MA^+$ ratio of 1 : 9 to 507 nm at the $OA^+ : MA^+$ ratio of 9 : 1 (Fig. 5d), again demonstrating the enhanced quantum confinement effect due to the increasing amount of long-chain OA^+. As for the absorption from nanoplatelets, while the intensity of the peak at around 430 nm from bi-layer nanoplatelets followed a decreasing trend, a new peak at 396 nm originated from monolayer nanoplatelets started to appear at $OA^+ : MA^+$ ratio of 4 : 6 and continued to increase with increasing OA^+ amount (Fig. 5c). Apparently, when $PbBr_2$ was used as lead source, nanoplatelets were always formed with varying $OA^+ : MA^+$ ratios, and more OA^+ tended to promote the growth of nanoplatelets with fewer layers. This is in agreement with the assumption that long-chain ammonium halide will cause the size reduction of perovskite NCs. For mono- and bi-layer nanoplatelets, their absorption peak positions kept generally constant in each sample (Fig. 5c), which indicates the thickness of these nanoplatelets was essentially unchanged. Interestingly, even though the absorption intensity from monolayer nanoplatelets was in dominance at higher $OA^+ : MA^+$ ratios, its corresponding PL emission at 403 nm was almost absent in these samples. It reveals that the monolayer nanoplatelets contribute much less to the overall PLQY of perovskite NCs. Tyagi *et al.* observed similar phenomenon that the absorbed energy downhill transferred from the blue-emitting monolayer nanoplatelets to the red-emitting thicker nanoplatelets.[16] Manser *et al.* suggested that the dominant relaxation pathway is recombination of free electrons and holes *via* femtosecond transient absorption spectroscopy measurements.[31] The recombination of thinner nanoplatelets with its inherently high surface to volume ratio will be lower because of exceptional sensitivity to surface defects.[31] Moreover, at an $OA^+ : MA^+$ ratio of 9 : 1, multiple absorption and PL emission peaks can be resolved and assigned to different number of nanoplatelet layers from 1 to 5 (Fig. S3†),

Table 1 Comparison of the absorption and PL peaks of 2D $CH_3NH_3PbBr_3$ nanoplatelets reported in ref. 12 and this work using Pb-oleate + $PbBr_2$ as lead source with $OA^+ : MA^+$ of 9 : 1

n^a	Abs (Ref) (nm)	Abs (Exp) (nm)	PL (Ref) (nm)	PL (Exp) (nm)
1	396	396	405	403
2	434	431	442	435
3	450	448	456	—
4	472	470	482	474
5	490	485	492	489
∞	532	—	534	508

[a] n represents the number of layers of nanoplatelets. When n approaches to ∞, the corresponding structure changes to nanoparticle formation.

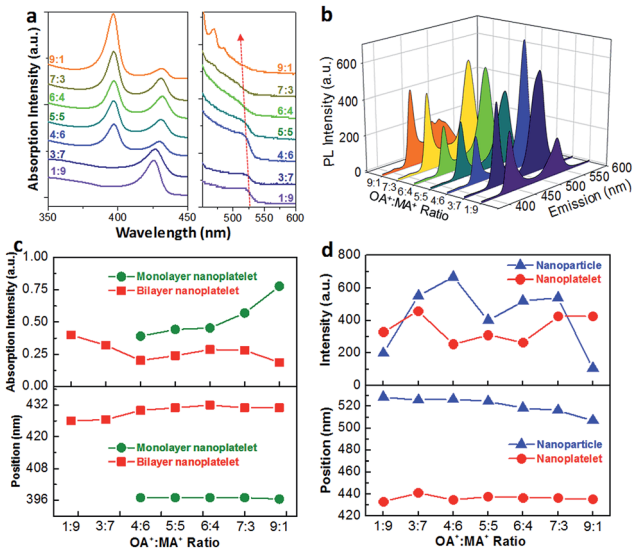

Fig. 5 Investigation of the impact of $OA^+ : MA^+$ ratios on the optical properties of the resulting $CH_3NH_3PbBr_3$ NCs solutions when using $PbBr_2$ + Pb-oleate as lead source. (a) UV-vis absorption curves of as-made $CH_3NH_3PbBr_3$ NCs solutions with varying $OA^+ : MA^+$ ratios. The curves were offset for better comparison. (b) PL emissions of as-made $CH_3NH_3PbBr_3$ NCs solutions with varying $OA^+ : MA^+$ ratios. The excitation wavelength was set as 350 nm. (c) The absorption peak intensity and position of mono- and bi-layer nanoplatelets from as-made $CH_3NH_3PbBr_3$ NCs solutions with varying $OA^+ : MA^+$ ratios. (d) The PL peak intensity and position of nanoplatelets and nanoparticles from as-made $CH_3NH_3PbBr_3$ NCs solutions with varying $OA^+ : MA^+$ ratios.

which is in agreement with reported values from ref. 12 (Table 1). The only absent emission peak of the tri-layer nanoplatelets may be due to interference by the adjacent strong peaks. The appearance of multiple PL emission peaks at higher $OA^+ : MA^+$ ratios indicates a weaker structure control of the grown perovskite NCs.

Conclusions

We developed a new strategy for controllable synthesis of monodispersed and stable $CH_3NH_3PbBr_3$ perovskite NCs using Pb-oleate as sole lead source. A series of control experiments were designed and revealed that the mole ratios of long- and short-chain alkyl ammonium halides ($OA^+ : MA^+$) in the precursors have a significant impact on the crystal shape of $CH_3NH_3PbBr_3$ NCs. At an optimal $OA^+ : MA^+$ ratio of 4 : 6, the growth of $CH_3NH_3PbBr_3$ NCs in the nanoplatelet shape is essentially suppressed, resulting in pure $CH_3NH_3PbBr_3$ perovskite nanoparticles with an average size of 2.2 nm and an improved photoluminescence quantum yield up to 85%. The result shown here provides important new insights for controlled synthesis of perovskite NCs with pure crystal shape and high quantum yield, paving the way for further applications of OHP NCs in optoelectronic devices.

Conflicts of interest

There are no conflicts of interest to declare.

Acknowledgements

Financial support from National Natural Science Foundation of China (Grant No. 51302096), China Scholarship Council (Grant No. 201606165006), the Fundamental Research Funds for the Central Universities (Grant No. 2015TS051), the Fundamental Research Funds of Wuhan City (Grant No. 2016060101010075), and the Innovation Foundation of Shenzhen Government (Grant No. JCYJ20160429182959405) are acknowledged. HLL acknowledges partial support from the National Key Research and Development Program of China (Grant No. 2016YFB0402705). YHW acknowledges partial support from AFOSR (Grant No. MURI FA9550-16-1-0150). The authors thank the Analytical and Testing Center of Huazhong University of Science and Technology and Maryland NanoCenter for making available the shared experimental facilities.

References

1 W. J. Yin, T. Shi and Y. Yan, *Adv. Mater.*, 2014, **26**, 4653–4658.
2 S. De Wolf, J. Holovsky, S.-J. Moon, P. Löper, B. Niesen, M. Ledinsky, F.-J. Haug, J.-H. Yum and C. Ballif, *J. Phys. Chem. Lett.*, 2014, **5**, 1035–1039.
3 H. Zhou, Q. Chen, G. Li, S. Luo, T. B. Song, H. S. Duan, Z. Hong, J. You, Y. Liu and Y. Yang, *Science*, 2014, **345**, 542–546.
4 V. D'Innocenzo, G. Grancini, M. J. Alcocer, A. R. S. Kandada, S. D. Stranks, M. M. Lee, G. Lanzani, H. J. Snaith and A. Petrozza, *Nat. Commun.*, 2014, **5**, 3586.
5 S. D. Stranks, G. E. Eperon, G. Grancini, C. Menelaou, M. J. Alcocer, T. Leijtens, L. M. Herz, A. Petrozza and H. J. Snaith, *Science*, 2013, **342**, 341–344.
6 G. Xing, N. Mathews, S. Sun, S. S. Lim, Y. M. Lam, M. Grätzel, S. Mhaisalkar and T. C. Sum, *Science*, 2013, **342**, 344–347.
7 A. Kojima, K. Teshima, Y. Shirai and T. Miyasaka, *J. Am. Chem. Soc.*, 2009, **131**, 6050–6051.
8 NREL, Best Research-Cell Efficiencies, https://www.nrel.gov/pv/assets/images/efficiency-chart.png, accessed 26 November 2017.
9 Y. Hassan, Y. Song, R. D. Pensack, A. I. Abdelrahman, Y. Kobayashi, M. A. Winnik and G. D. Scholes, *Adv. Mater.*, 2016, **28**, 566–573.
10 G. C. Papavassiliou and I. Koutselas, *Synth. Met.*, 1995, **71**, 1713–1714.
11 G. C. Papavassiliou, *Prog. Solid State Chem.*, 1997, **25**, 125–270.
12 C. Kagan, D. Mitzi and C. Dimitrakopoulos, *Science*, 1999, **286**, 945–947.
13 K. Chondroudis and D. B. Mitzi, *Chem. Mater.*, 1999, **11**, 3028–3030.
14 L. C. Schmidt, A. Pertegás, S. González-Carrero, O. Malinkiewicz, S. Agouram, G. Minguez Espallargas, H. J. Bolink, R. E. Galian and J. Pérez-Prieto, *J. Am. Chem. Soc.*, 2014, **136**, 850–853.
15 P. Tyagi, S. M. Arveson and W. A. Tisdale, *J. Phys. Chem. Lett.*, 2015, **6**, 1911–1916.
16 Y. Ling, Z. Yuan, Y. Tian, X. Wang, J. C. Wang, Y. Xin, K. Hanson, B. Ma and H. Gao, *Adv. Mater.*, 2016, **28**, 305–311.
17 J. A. Sichert, Y. Tong, N. Mutz, M. Vollmer, S. Fischer, K. Z. Milowska, R. García Cortadella, B. Nickel, C. Cardenas-Daw and J. K. Stolarczyk, *Nano Lett.*, 2015, **15**, 6521–6527.
18 S. Pathak, N. Sakai, F. Wisnivesky Rocca Rivarola, S. D. Stranks, J. Liu, G. E. Eperon, C. Ducati, K. Wojciechowski, J. T. Griffiths and A. A. Haghighirad, *Chem. Mater.*, 2015, **27**, 8066–8075.
19 F. Zhang, H. Zhong, C. Chen, X.-g. Wu, X. Hu, H. Huang, J. Han, B. Zou and Y. Dong, *ACS Nano*, 2015, **9**, 4533–4542.
20 S. Gonzalez-Carrero, R. E. Galian and J. Pérez-Prieto, *J. Mater. Chem. A*, 2015, **3**, 9187–9193.
21 Y. Shirasaki, G. J. Supran, M. G. Bawendi and V. Bulović, *Nat. Photonics*, 2013, **7**, 13–23.
22 S. Ahmad, P. K. Kanaujia, W. Niu, J. J. Baumberg and G. Vijaya Prakash, *ACS Appl. Mater. Interfaces*, 2014, **6**, 10238–10247.
23 Y. Tabuchi, K. Asai, M. Rikukawa, K. Sanui and K. Ishigure, *J. Phys. Chem. Solids*, 2000, **61**, 837–845.
24 M. C. Weidman, M. Seitz, S. D. Stranks and W. A. Tisdale, *ACS Nano*, 2016, **10**, 7830–7839.
25 G. C. Papavassiliou, G. Pagona, N. Karousis, G. A. Mousdis, I. Koutselas and A. Vassilakopoulou, *J. Mater. Chem.*, 2012, **22**, 8271–8280.

26 Z. Yuan, Y. Shu, Y. Xin and B. Ma, *Chem. Commun.*, 2016, **52**, 3887–3890.
27 H. Huang, F. Zhao, L. Liu, F. Zhang, X.-g. Wu, L. Shi, B. Zou, Q. Pei and H. Zhong, *ACS Appl. Mater. Interfaces*, 2015, **7**, 28128–28133.
28 D. H. Cao, C. C. Stoumpos, O. K. Farha, J. T. Hupp and M. G. Kanatzidis, *J. Am. Chem. Soc.*, 2015, **137**, 7843–7850.
29 S. Gonzalez-Carrero, G. M. Espallargas, R. E. Galian and J. Pérez-Prieto, *J. Mater. Chem. A*, 2015, **3**, 14039–14045.
30 J. S. Manser and P. V. Kamat, *Nat. Photonics*, 2014, **8**, 737–743.
31 Y. Bekenstein, B. A. Koscher, S. W. Eaton, P. Yang and A. P. Alivisatos, *J. Am. Chem. Soc.*, 2015, **137**, 16008–16011.